HHS Public Access

Author manuscript

Cell. Author manuscript; available in PMC 2020 February 21.

Published in final edited form as:

Cell. 2019 February 21; 176(5): 1128–1142.e18. doi:10.1016/j.cell.2018.12.023.

A unique collateral artery development program promotes neonatal heart regeneration

Soumyashree Das[1,#], **Andrew B. Goldstone**[2,#], **Hanjay Wang**[2], **Justin Farry**[2], **Gaetano D'Amato**[1], **Michael J. Paulsen**[2], **Anahita Eskandari**[2], **Camille E. Hironaka**[2], **Ragini Phansalkar**[1,5], **Bikram Sharma**[6], **Siyeon Rhee**[1], **Elya Ali Shamskhou**[4], **Dritan Agalliu**[7], **Vinicio de Jesus Perez**[4], **Y. Joseph Woo**[2,*], and **Kristy Red-Horse**[1,3,8,*]

[1]Department of Biology, Stanford University, Stanford, California 94305, USA

[2]Department of Cardiothoracic Surgery, Stanford University School of Medicine, Stanford, California 94305, USA

[3]Institute for Stem Cell Biology and Regenerative Medicine, Stanford University School of Medicine, Stanford, California, 94305, USA

[4]Department of Medicine, Stanford University School of Medicine, Stanford, California 94305, USA

[5]Department of Genetics, Stanford University, Stanford, California 94305, USA

[6]Department of Biology, Ball State University, Muncie, Indiana 47306, USA

[7]Departments of Neurology, Pathology and Cell Biology, Pharmacology, Columbia University Irving Medical Center, New York, 10032, USA

[8]Lead Contact

Summary

Collateral arteries are an uncommon vessel subtype that can provide alternate blood flow to preserve tissue following vascular occlusion. Some patients with heart disease develop collateral coronary arteries, and this correlates with increased survival. However, it is not known how these collaterals develop or how to stimulate them. We demonstrate that neonatal mouse hearts use a

For correspondence, please contact Kristy Red-Horse Ph.D. kredhors@stanford.edu or Y. Joseph Woo M.D. joswoo@stanford.edu.

[#]These authors contributed equally

[*]These authors contributed equally

Author Contributions:

S.D., A.B.G., Y.J.W. and K.R-H. conceptualized the study. V.J.P., Y.J.W. and K.R-H provided resources. D.A. provided *Tie2::eGFP::Claudin5* mouse line. S.D., A.B.G. and K.R-H. designed the experiments and analyzed the results. S.D., A.B.G., Y.J.W., and K.R-H. wrote and or edited manuscript. S.D. performed the majority of experiments. A.B.G. and H.W. performed coronary ligations in neonatal and adult mice. J.F. collected confocal images of adult hearts. G.D. performed apical resections. M.J.P. contributed to coronary ligations in adult mice. A.E. performed adult cardiac function analyses. B.S., S.R. and R.P. contributed to data analysis. C. E.H. and E.A.S. provided technical support.

Declaration of Interests:

Authors declare no competing interests.

novel mechanism to build collateral arteries in response to injury. Arterial endothelial cells (ECs) migrated away from arteries, along existing capillaries, and reassembled into collateral arteries, which we termed Artery Reassembly. Artery ECs expressed CXCR4, and, following injury, capillary ECs induced its ligand, CXCL12. CXCL12 or CXCR4 deletion impaired collateral artery formation and neonatal heart regeneration. Artery Reassembly was near absent in adults, but was induced by exogenous CXCL12. Thus, understanding neonatal regenerative mechanisms can identify pathways that restore these processes in adults and identify potentially translatable therapeutic strategies for ischemic heart disease.

Graphical Abstract

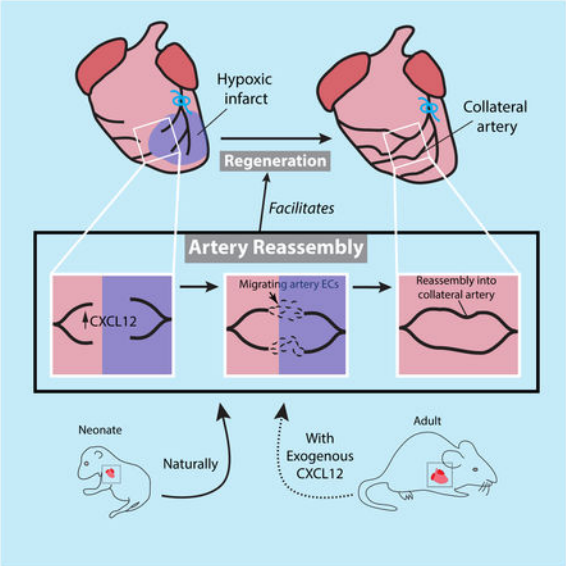

Introduction

Coronary artery disease (CAD) is a leading cause of death worldwide because it obstructs essential blood flow to heart muscle, resulting in cardiac ischemia or myocardial infarction (MI) (Go et al., 2014). Revascularization can be achieved through stenting and coronary artery bypass grafting, but many patients are not amenable to these therapies, thus calling for new approaches (Seiler et al., 2013). One alternative could be induction of a unique artery subtype called collateral arteries. These arterial segments bridge two conventional arteries, forming a natural bypass that restores blood flow downstream of an obstruction. In fact, patients with significant collateral coronary arteries can survive with normal heart function despite one or two completely occluded native coronary arteries (Habib et al., 1991; Hara et al., 2016; Helfant et al., 1971; Kim et al., 2016; Meier et al., 2014). It is not known how collateral arteries arise in humans, but knowledge of the process could guide efforts to induce them as an alternative revascularization therapy (Zimarino et al., 2014).

Studies primarily in the mouse brain and hind limb have described two mechanisms by which collateral arteries form (Faber et al., 2014; Simons and Eichmann, 2015). The first is Arterialization, or the transformation of capillaries into arteries. The second is

Arteriogenesis, or the widening of pre-existing collateral arteries. Although many studies have addressed conventional artery growth in the injured mouse heart (He et al., 2017; Ingason et al., 2018; Lavine et al., 2013; Miquerol et al., 2015; Tang et al., 2018), there is little knowledge on which mechanism produces true collateral arteries following ischemic injury.

Our lack of knowledge is partially due to the absence of unique markers—their only defining feature is that collaterals bridge two conventional arteries. Thus, three-dimensional, whole mount imaging is required to identify this vessel subtype. Tissue sections are not sufficient. Previous lineage tracing has suggested that Arteriogenesis forms collateral arteries in response to heart injury (He et al., 2016); however, others report that there are no pre-existing collaterals in mouse hearts to undergo Arteriogenesis (Zhang and Faber, 2015). Furthermore, the lineage tracing study did not observe lineage labeling in whole mount preparations to confirm collateral identity. The authors also concluded that their techniques could not analyze small caliber arteries (He et al., 2016). This is important because whole mount observations have shown that collateral coronary arteries connect smaller branches of non-injured and obstructed arteries, and this occurs at sites bordering the ischemic myocardium (Hagensen et al., 2008; He et al., 2016; Porrello et al., 2013; Zhang and Faber, 2015). Therefore, a precise picture on how collateral arteries of the mouse heart arise remains an unanswered question.

Although the adult mammalian heart cannot regenerate, the neonatal mouse heart can repair itself when injury is performed within the first days of life (Haubner et al., 2012, 2016; Porrello et al., 2013). Heart muscle cannot survive without vascularization, suggesting that neonates establish collateral arteries early in regeneration. Corrosion casting showed a collateral artery network at 21 days post-MI when injury was performed at postnatal day 1 (P1) (Porrello et al., 2013). However, no study has addressed the developmental sequence, inductive signals, or functional significance of the collateral arteries that develop following neonatal MI.

By combining whole-organ imaging with lineage tracing and mouse genetics, we found that the neonatal heart uses a unique mechanism to form a collateral artery network that facilitates regeneration. Our data support a model where neonatal injury activates CXCL12 expression in capillary endothelial cells, stimulating arterial endothelial cell (EC) migration and expansion along the capillary network and their subsequent reassembly into collateral arteries. This developmental sequence is specific to the regenerative window in mice, and required for neonatal heart regeneration, but can be reactivated in adults through application of exogenous CXCL12.

Results

To analyze collateral artery formation during neonatal heart regeneration, we developed a method to image coronary arteries—at the cellular level—in the intact heart. Neonates were subjected to experimental MI through permanent ligation of the left coronary artery (LCA) and then whole-heart confocal microscopy. Ligating the LCA at P2 (Figure S1A) completely interrupted blood flow (Figure S1B), but, as reported (Haubner et al., 2012, 2016; Porrello et

al., 2013), ultimately resulted in significant regeneration (Figure S1C). To visualize arteries, MIs were performed in *Cx40CreER* and *Rosa26*^{TdTomato} animals where Connexin40^{+} (CX40) arterial ECs could be marked with red fluorescence. These animals expressed TdTomato in arterial ECs upon Tamoxifen injection (recombination efficiency, 84%) (Figure S1D and E). This experimental set up was used to investigate collateral artery formation in the injured neonatal heart (Figure 1A).

Whole mount confocal imaging of the entire organ 4 days post-MI revealed numerous collateral arteries, particularly in the watershed area. A watershed area is a region that receives blood from distal branches of two large arteries. The capillary network at the anterior midline of the heart is a watershed because it receives blood from left and right coronary artery branches (Figure 1B). In control and sham operated animals, no arteries spanned the watershed area (Figure 1C). In contrast, MI hearts contained *Cx40CreER*-labeled collateral arteries spanning the watershed to connect distal branches of the ligated LCA with the non-ligated right coronary artery (Figure 1D and Figure S2A). Similar observations were made using whole mount immunofluorescence for CX40 (Figure S2B-D). MI also induced organ-wide extension of artery tips (Figure 1D and Figure S2E and F), but it only changed capillary density within ischemic zones where it was decreased (Figure S2G). Thus, a neonatal MI stimulated the de novo appearance of collateral arteries within days post injury. In theory, these vessels could provide blood flow to vessels downstream of the occlusion (Figure 1E).

We next characterized and quantified features of these early collateral arteries. Two types were observed: (1) connections between branches of the right and left coronary arteries across the watershed (Right-to-Left collaterals) (Figure 1D and Figure S2A and C), and (2) connections between the ligated and non-ligated branches of the LCA (Left-to-Left collaterals)(Figure S2D). Both types were anastomoses between the distal-most branches of their respective arteries and were only seen between a ligated and non-ligated vessel. Smooth muscle covered a subset of collateral arteries at 4 days post ligation (Figure 1F). Quantification revealed an average of 10 *Cx40CreER*-labeled collateral arteries per heart (Figure 1G), a subset of which were covered by smooth muscle (Figure 1H). Collaterals were still present at 10 days after injury (Figure S2H). The average caliber at 4 days post MI was similar to the distal-most (4°) branches of non-injured arteries, which is consistent with their bridging of two artery tips (Figure 1I). Injecting fluorescently-labeled Lectin showed that collaterals were perfused with blood (Figure 1J). Thus, MI induces a large number of functional collateral arteries in the neonatal heart, mostly in the watershed region, but also around the ligation site.

Since the majority of collateral arteries appeared in the watershed where there were no pre-existing collaterals, we hypothesized that they developed through Arterialization, or the transformation of capillaries into arteries (Simons and Eichmann, 2015). This possibility was tested through capillary EC lineage tracing using the *ApjCreER* allele (Chen et al., 2014) and the *Rosa26*^{TdTomato} Cre reporter. Lineage-labeling was induced at P0 by injecting Tamoxifen into mothers, and resulted in TdTomato expression specifically in capillaries and veins with 86% recombination efficiency (Figure S3A). Then, neonates underwent MI at P2. Collateral arteries were analyzed 4 days later through CX40 immunofluorescence (Figure

2A). Unexpectedly, few *ApjCreER*-labeled cells were present in collateral arteries (Figure 2B and Figure S3B), showing that collaterals forming in neonates are not derived from Arterialization.

We next investigated whether arterial ECs formed collaterals. Arterial ECs were lineage-labeled at P0 by injecting Tamoxifen into *Cx40CreER; Rosa26*^{TdTomato} transgenic mice (Figure 2A). Here, CX40^{+} collaterals were primarily composed of *Cx40CreER* lineage labeled cells (Figure 2C and Figure S3C). Quantification confirmed they were primarily derived from pre-existing arterial endothelial cells, and not capillaries (Figure 2D). This result was not due to persistence of Tamoxifen in the mother; there was no lineage labeling when transgenic pups were transferred to injected females 2 days after injection (Figure S3D-G). Underscoring the unique nature of collateral arteries, their origins were different from normal postnatal artery growth, which we observed to be through capillary Arterialization at vessel tips (Figure S3H-J). In summary, neonatal collateral artery development is distinct from Arterialization because they arise from an arterial source, and distinct from Arteriogenesis because they appear where pre-existing collateral arteries are absent.

It was next investigated whether this robust collateral artery development program was specific to the neonatal regenerative period, which is the first few days of life (Haubner et al., 2012, 2016, Porrello et al., 2011, 2013). Artery cells were lineage labeled and MIs were performed at either P2 (within regenerative period) or P7 (non-regenerative period). Strikingly, while P2 injured watershed areas were filled with arterial cells and collateral arteries (Figure 3A-C), hearts injured at P7 were devoid of these features (Figure 3D-F). We next assessed vascular perfusion of the infarct following MI at both time points. Injecting fluorescent Lectin and measuring fluorescence intensity indicated that perfusion was higher 4 days post-MI when the injury was performed at P2 compared to P7 (Figure 3G and H). These results show that collateral artery development in neonates (as observed with arterial lineage tracing) is correlated with both the neonatal regenerative window and increased reperfusion of ischemic myocardium.

Next, we investigated the cellular mechanism by which arterial cells create collaterals. One clue came from observations of injured hearts with arterial lineage labeling. The watershed regions contained numerous non-coalesced, lineage-labeled ECs that bridged two artery tips (Figure 3B and C). We hypothesized that these cells represented an intermediate state of collateral formation. To explore this hypothesis, we examined earlier time points and analyzed EC morphology at higher magnification. At 6 hours post-MI, the arterial ECs of the ligated vessel appeared similar to controls (Figure 4A and B). At 24 hours, collaterals had not yet formed, but cells at artery tips had filopodia-like structures (Figure 4C), and single arterial ECs had moved into the watershed (Figure S4A). At 4 days, collateral arteries were present and arterial tips that had not formed collaterals were even more mobilized (Figure 4D and E, Figure S4B). This was observed in both the ligated and non-ligated arteries. Artery ECs generally do not proliferate (Su et al., 2018). However, EdU labeling revealed that individual artery ECs in the watershed proliferated at rates similar to capillary ECs (Figure 4F). ECs that become part of a collateral artery are no longer proliferative (Figure 4F). Although we cannot perform time-lapse imaging of the mammalian heart, time

course, lineage, and proliferation data suggested that, upon injury, arterial ECs migrate out of their resident vessels and proliferate before coalescing into non-proliferative collateral arteries.

To explore the migratory path of artery ECs in response to injury, we crossed *Cx40CreER; Rosa26*^{TdTomato} mice with those containing a *Tie2*::*eGFP::Claudin5* allele, which labels all endothelial cell-cell junctions with eGFP (Knowland et al., 2014; Lutz et al., 2017). Following MI, single artery cells in the watershed were positioned along capillaries (Figure 4G-J). Orthogonal sections revealed in >90% of the cells were part of the capillary endothelial layer, directly lining the capillary lumen (Figure 4J, K, L). Taken together, the above data suggests that, upon coronary ligation, single arterial ECs migrate as part of the capillary endothelial layer and then coalesce with each other to make collateral arteries. This is distinct from current models of collateral artery formation and we, therefore, termed it "Artery Reassembly" (Figure 4M).

Regeneration also occurs when the apex of the neonatal heart is resected (Porrello et al., 2011). The injury is different than MI since it severs artery tips instead of blocking blood flow through one side of the coronary tree. Arterial EC lineage tracing after P2 apical resection showed a similar response as MI. Although watershed areas from apices of sham-operated hearts were devoid of arteries (Figure S4C, D), the right and left coronary artery branches of resected hearts were connected through *Cx40CreER* lineage-labeled collateral arteries (Figure S4E). These connected arteries in the regenerating apex with those of adjacent non-resected tissue. The resected watershed areas were also occupied by single artery-derived ECs surrounding the collaterals (Figure S4E). We concluded that Artery Reassembly also occurs in response to apical resection.

We next hypothesized that migrating artery cells would be attracted by signals from capillary endothelial cells. The chemotactic ligand, *Cxcl12*, is important for guiding coronary ECs migration during embryonic development (Cavallero et al., 2015; Chang et al., 2017; Ivins et al., 2015). In non-injured neonatal hearts, *Cxcl12* was expressed mostly in arterial ECs, as assessed by the *Cxcl12-DsRed* reporter mouse (Figure S5A and B). However, as early as 24 hours post-MI, it was induced in capillary ECs of the watershed area (capillary defined as Lectin perfused, CX40 negative, small diameter) (Figure 5A-C and Figure S5C). The CXCL12 receptor, CXCR4, was specifically expressed in arterial ECs both pre- and post-MI (Figure S5A and data not shown). Notably, CXCR4 was expressed in coronary artery specimens from patients, increasing the prospective relevance of this pathway (Figure S5D). Thus, the spatiotemporal expression of CXCL12 and CXCR4 suggested a potential function in guiding artery cell migration during collateral development.

CXCL12 is upregulated by hypoxia in other settings (Baxter et al., 2008; Ceradini et al., 2004; Hitchon et al., 2002; Kryczek et al., 2005; Tabatabai et al., 2006), suggesting that the hypoxic environment created post-MI could trigger CXCL12 induction. To test this, P0 *Cxcl12-DsRed* neonates, along with their mothers, were placed in chambers with low oxygen (10%) for 4 days before assessing *Cxcl12* expression. *Cxcl12-DsRed* was specific to arteries in normoxic hearts, and there was a clear watershed area (Figure 5D). In contrast, hypoxia-treated hearts contained *Cxcl12-DsRed* signal in watershed regions throughout the

heart (Figure 5E and Figure S5E) in a pattern similar to MI hearts, i.e. in capillaries bridging two artery tips (Figure 5C). In MI hearts, we would anticipate *Cxcl12-DsRed* induction to be restricted to the injury site if hypoxia were the trigger. Indeed, capillary *Cxcl12-DsRed* was observed in the watershed regions adjacent to the infarct, but not in remote zones, following MI (Figure S5F). In further support of CXCL12 stimulating arterial migration, the lack of *Cxcl12-DsRed* induction in remote areas correlated with a decrease in single cell migration from the arteries (Figure S5F and G). These data support the notion that MI-induced hypoxia is the stimulus that increases *Cxcl12* in capillary ECs in response to injury.

We next performed gene deletion experiments to test the role of this signaling axis. *Cxcl12* or *Cxcr4* were deleted from either artery cells using *Cx40CreER* or all ECs using *Cdh5CreER* by injecting Tamoxifen at P0. MI was performed at P2, and hearts were analyzed at P6 for the number of collateral arteries using CX40 immunofluorescence. Deleting *Cxcl12* in artery cells alone did not affect collateral formation (Figure 5F). In contrast, its removal from all ECs decreased collateral numbers (Figure 5G and Figure S6A). This indicated that capillary CXCL12, instead of arterial CXCL12, is required for collateral development. Deleting *Cxcr4* in artery cells was sufficient to inhibit both artery cell migration into the watershed area (Figure 5H-J) and collateral formation (Figure 5H, I, K and L). The above results were not secondary to baseline coronary defects caused by *Cxcl12* or *Cxcr4* deletion since without MI there were no gross abnormalities (Figure S6B and C). The depletion of CXCR4 protein was robust (Figure S6D), although a lack of immunofluorescence-compatible CXCL12 antibodies precluded investigating its protein levels. The absence of a baseline phenotype is likely because of postnatal deletion when the coronary vasculature is already formed. Previous studies that affected coronary vessels removed the genes during early development (Cavallero et al., 2015; Harrison et al., 2015; Ivins et al., 2015). The CXCL12/CXCR4 expression patterns in the injured heart and EC subtype specific deletions support the following model: upon injury, induction of capillary CXCL12 attracts CXCR4-expressing artery cells out from arteries and into the watershed, where they subsequently proliferate and reassemble into collateral arteries (Figure 6A).

Given that Artery Reassembly was specific to the regenerative window, we assessed whether it contributed to neonatal heart regeneration. MIs were performed at P2 in the conditions that inhibited collateral artery development, but instead of analyzing hearts 4 days post-MI, animals were assessed for heart function and fibrosis 28 days post-injury. As reported (Haubner et al., 2012, 2016; Porrello et al., 2013), heart function as measured by ejection fraction was normal when control animals were injured, indicating functional recovery and regeneration (Figure 6B). In contrast, deletion of *Cxcl12* in all ECs or *Cxcr4* in arterial ECs decreased ejection fraction (Figure 6C and D). These deletions did not have a baseline effect without injury (Figure 6E). Masson's Trichrome staining to assess fibrosis showed an increase in scarring in both cases (Figure 6F and Figure S6E). Cardiomyocyte proliferation 7 days post-MI was also decreased in both knockouts (Figure 6G and H). We also noted that *Cxcr4* deletion decreased artery tip expansion in all regions of the heart (Figure S2F). However, blood flow directly into ligated arteries through collaterals is likely to be more beneficial than distant tip expansion in remote zones during regeneration (Figure S2G). These data indicate that endothelial CXCL12-CXCR4 signaling facilitates Artery

Reassembly into collateral arteries and support a model where collateral development is required for the full regenerative response (Figure 6A).

Artery Reassembly did not occur in P7 hearts, prompting us to investigate whether applying CXCL12 could induce the process in adults. Adult hearts are much larger and more difficult to image in whole mount. Therefore, we first captured low-resolution images of the entire heart with a fluorescent stereomicroscope before separating the heart into anterior and posterior halves and subjecting them to confocal microscopy (Figure 7A-C). For each anterior wall—which contains the watershed region between the right and left coronary arteries—tiled, high-resolution confocal images of the entire region were reconstructed and assessed for artery lineage labeled collaterals (Movies S1 and S2). In line with previous data (Zhang and Faber, 2015), hearts did not have pre-existing $CX40^{+}$ collateral arteries without MI (Figure 7A-C). Similar to MI at P7 (Figure 3D and E), injured adult hearts almost never formed artery-derived collaterals through the Artery Reassembly process, even after 30 days post-injury (Figure S7A-C).

We next investigated whether exogenous CXCL12 could stimulate Artery Reassembly in adults. A single dose of CXCL12 was injected into the watershed area of *Cx40CreER; Rosa26*^{TdTomato} adult hearts at the time of MI. At 4 days post-MI, CXCL12 did not stimulate any artery-derived collaterals (Figure 7D-J). However, at 14 days post-MI, CXCL12-treated hearts contained numerous collaterals connecting left and right artery branches across the watershed region (Figure 7J, K and Figure S7D, E). Nearly all PBS-treated hearts lacked these vessels (Figure 7J and Movie S1). We have recently shown that a CXCL12 injection protocol similar to that used here enhances cardiac recovery post-MI (Goldstone et al., 2018), which replicates previous findings, but the mechanism of action, i.e. the signal-receiving cells mediating cardioprotection, is still under debate (Askari et al., 2003; Macarthur et al., 2014; Penn et al., 2012; Saxena et al., 2008; Sundararaman et al., 2011). The data shown here suggest that part of the beneficial response to CXCL12 could be stimulation of artery-derived collateral arteries. Why neonate, P7, and adult arterial responses differ is not clear. Published transcriptional analyses listed *Cxcl12* as being downregulated in adult cardiac ECs when compared to neonates post-injury (Quaife-Ryan et al., 2017). We observed capillary induction of *Cxcl12-DsRed* at P7 post-MI indicating that loss of CXCL12 expression does not explain the loss of Artery Reassembly at this time (Figure S7F). Although, the *Cxcl12-DsRed* reporter may not be quantitative. Furthermore, CXCL12/CXCR4 signaling is complex, containing multiple negative regulators. Dynamics of all the molecular players may underlie changes between P2 and P7. Our data show that any changes can be overcome in adults with a high dose of exogenous CXCL12.

Discussion

The mammalian heart's transient capacity to repair itself during the neonatal period is a recent discovery (Haubner et al., 2012, 2016, Porrello et al., 2011, 2013), and knowledge on this could identify treatments that stimulate healing in the adult (Tzahor and Poss, 2017). Much attention is paid to the increased ability of neonatal cardiomyocytes to proliferate. Here, we show that neonatal coronary arteries also have special reparative properties. During the neonatal regeneration period, arterial EC lineage labeling showed the appearance of

proliferative single artery-derived ECs in the watershed area and around the ligation site post-injury. Subsequently, collateral arteries that connected non-injured and obstructed arteries appeared. The single artery-derived ECs were along capillaries that induced *Cxcl12* upon MI. Collateral development was inhibited upon endothelial *Cxcl12* or arterial *Cxcr4* deletion, as was heart regeneration. Finally, one dose of CXCL12 at the time of MI stimulated this collateral development process in adults. These data indicate that neonatal arterial ECs are attracted by capillary CXCL12 to the watershed area where they expand and then establish a collateral artery network. This response can be reactivated in adults upon CXCL12 injection.

We found that the $CX40^{+}$ neonatal collateral artery network developed through mechanisms distinct from those described to date. Instead of widening of pre-existing collaterals (Arteriogenesis) (He et al., 2016) or Arterialization (Gabhann and Peirce, 2010), neonatal hearts utilize a completely different third cellular process that is a hybrid of the two. This is a hybrid because, like Arteriogenesis, the collateral artery is formed using pre-existing artery cells, but, like Arterialization, this new collateral artery is formed where a capillary existed before injury. We refer to this as Arterial Reassembly. It is likely that Artery Reassembly is not the only method of constructing collateral arteries in the heart. Collateral arteries, as defined by microfil injection experiments, have been found in adult hearts within days of MI (Zhang and Faber, 2015). However, our lineage data indicate that Artery Reassembly would not form these collaterals. Identification of this new cellular process will facilitate discovery of its regulatory mechanisms.

CXCL12 is known to limit infarct size and improve cardiac function post-MI (Askari et al., 2003; Hiesinger et al., 2011; Macarthur et al., 2014; Penn et al., 2012; Sundararaman et al., 2011), but its mechanism of action is poorly understood. It may recruit angiogenic cells from the bone marrow (Abbott et al., 2004; Saxena et al., 2008; Segers et al., 2007), or it may affect cardiomyocytes directly (Dong et al., 2012; Hu et al., 2007). Our data suggests that collateral artery formation contributes to the functional benefit of CXCL12 injection. Exogenous CXCL12 induced dramatic expansion of artery ECs. It is possible that this expansion itself results in collateral artery assembly. This is consistent with unpublished data from our laboratory showing that increased artery cell differentiation leads to collateral formation. However, additional roles for hematopoietic cells in collateral formation remain possible. Particularly in light of previous studies showing the importance of hematopoietic cells during cardiac injury and regeneration (Aurora et al., 2014). CXCL12 enhancing the injury response through pleotropic beneficial mechanisms may increase its desirability as a human therapeutic target.

Genetic evidence suggests that altered CXCL12 correlates with human CAD. Genome-wide association studies have detected CAD associated SNPs near the *Cxcl12* gene (Samani et al., 2007; Schunkert et al., 2011) and these SNPs are also associated with changes in serum protein levels (Ghasemzadeh et al., 2015; Kiechl et al., 2010; Mehta et al., 2011, 2014). The Reilly laboratory reported an increase in CXCL12 serum levels in CAD patients with the disease associated SNP (Mehta et al., 2011, 2014). How this chronic organismal level alteration would affect ECs within the myocardium exposed to acute injury would be an important line of investigation, as would whether mouse and human cells respond similarly.

The accumulated data suggesting a role for CXCL12 in mouse and human CAD has led to human trials (Döring et al., 2014; Ziff et al., 2018). A human trial of a naked DNA plasmid encoding CXCL12 failed to demonstrate significant clinical efficacy, possibly due to delivery mechanisms (Penn et al., 2012; Sundararaman et al., 2011). With the mechanistic information shown here, one could envision altering delivery strategies by targeting CXCL12 to ECs in the watershed area in ischemic heart disease patients to stimulate collateral formation as a preventative therapy or as a therapy at the time of MI.

Collateral arteries are observed in up to one-third of human patients with CAD. Unlike mice, a subset of the human population may have small, pre-existing collaterals, although there are no experiments to confirm this (Meier et al., 2013; Wustmann et al., 2003). Larger collateral arteries are observed in diseased hearts, but whether they arise de novo from artery tips—as we observe in the mouse—or from remodeling of potential pre-existing collaterals is not known. Interestingly, mature human collaterals resemble the artery-derived collaterals we found in mice; they span watershed areas between the right and left coronary artery, or between posterolateral and anterior branches of the left coronary artery (Seiler et al., 2013). Thus, our data provide mechanistic insight into how collateral coronary arteries can form de novo, and hopefully will inform the advent of novel treatments for humans with coronary artery disease.

STAR METHODS

CONTACT REAGENT AND RESOURCE SHARING

Further information and requests for resources and reagents should be directed to and will be fulfilled by the Lead Contact, Kristy Red-Horse (kredhors@stanford.edu).

EXPERIMENTAL MODELA ND SUBJECT DETAILS

Mice—All mouse colonies were housed and bred in the animal facility at Stanford University in accordance with institutional animal care and use committee (IACUC) guidance. All mouse lines were described earlier: *Cx40CreER* (Miquerol et al., 2015), *ApjCreER* (Chen et al., 2014), *Tie2::eGFP::Claudin5* (Knowland et al., 2014; Lutz et al., 2017). *Cdh5CreER* transgenic mice (Wang et al., 2010). *Cxcl12*$^{fl/fl}$ (The Jackson Laboratory, B6(FVB)-*Cxcl12*$^{tm1.1Link}$/J, Stock# 021773), *Cxcr4*$^{fl/fl}$ (The Jackson Laboratory, B6.129P2-*Cxcr4*^{tm2Yzo}/J, Stock# 008767), *Rosa26*^{TdTomato} Cre reporter (The Jackson Laboratory, B6.Cg-*Gt(ROSA)26Sor*$^{tm9(CAG-TdTomato)Hze}$/J, Stock# 007909) *Rosa26*^{Zsgreen} (The Jackson Laboratory, B6.Cg-*Gt(ROSA)26Sor*$^{tm6(CAG-zsGreen1)Hze}$/J, Stock# 007906), and *Cxcl12-DsRed* (The Jackson Laboratory, *Cxcl12*$^{tm2.1Sjm}$/J, Stock# 022458). For neonatal studies, all Tamoxifen injections to activate Cre activity (6mgs in corn oil) were given intraperitoneally to nursing mothers. Due to mouse genetic inheritance, analyses were compiled from age-matched males and females from multiple litters.

METHOD DETAILS

All procedures were performed under protocols approved by the Stanford University IACUC.

Neonatal LCA ligations—Procedure was modified from Mahmoud et al. (Mahmoud et al., 2014). P2 or late P7 neonates were cooled on ice for 6 minutes to induce hypothermic circulatory arrest and placed in a supine position followed by prepping with ethanol. Left anterolateral thoracotomy was made under dissecting microscope guidance. Dissection was carried through the pectoralis major and minor muscles, and the thoracic cavity was entered via the 4th intercostal space. The left coronary artery was identified and ligated using 6-0 prolene suture. The chest was then closed in layers with interrupted 6-0 prolene sutures. The neonate was then allowed to recover at 37°C warm plate and, when conscious, returned to its mother's care. Due to mouse genetic inheritance, values for each parameter were compiled from both males and females from multiple litters. The validity of this approach was confirmed with comparisons of non-injured mutants and injured versus control wild-type animals, which were not significantly different.

Adult LCA ligations—Mice were initially placed in 1.5-4% isoflurane chamber for induction. Once sedated but still with spontaneous respirations, the mice were intubated with a 20G angiocatheter and maintained on 1.5-4% isoflurane under mechanical ventilation at a respiratory rate of 180. The mice were then positioned for a left thoracotomy and the surgical site was shaved and prepped. 1-2mg/kg Bupivicaine and 0.5-1mg/kg Buprenorphine were injected subcutaneously at the pre-incision site. A 1cm incision was made to enter the left chest, the pericardium reflected, and 8-0 polypropylene suture was placed around the main branch of the LCA. In cases where CXCL12 was applied, 40μL of either 6μg/kg of CXCL12 (R&D System; Cat: 460-SD/CF) diluted in phosphate buffered saline (PBS) or vehicle only was injected intramyocardially into the borderzone/watershed area. In all cases, the chest was then closed in layers, first closing the thoracic cavity with a 5-0 polypropylene suture and then the skin with another 5-0 polypropylene suture. Isoflurane was then weaned to 0%. Once the mouse regained its physiological respirations and was awake, it was extubated. 5mg/kg Carprofen was injected subcutaneously into the mice every 24 hours for the first three days post-surgery.

For Lectin perfusions, prior to harvesting hearts, 50μl of 0.25μg/μl fluorescently labeled Lectin (Vector Laboratories; Cat: DL-1178) was circulated in the vasculature by intrajugular injections.

Neonatal apical resections—Procedure was modified from Mahmoud et al. (Mahmoud et al., 2014). Neonates were cooled on ice for 6 minutes to induce hypothermic circulatory arrest and placed in a supine position followed by prepping with ethanol. Left anterolateral thoracotomy was made under dissecting microscope guidance. Dissection was carried through the pectoralis major and minor muscles, and the thoracic cavity was entered via the 4th intercostal space. Apical resection of ~15% of the left ventricle was performed. Post-resection, a 6-0 suture was used to suture the ribs back together, reseal the chest wall and rejoin the skin. The neonate was then allowed to recover at 37°C warm plate and, when conscious, returned to its mother's care.

Echocardiography—Left ventricular geometry and function were evaluated 4 weeks after MI with high resolution (30MHz) Vevo 2100 transthoracic echocardiography system (VisualSonics, Toronto, Canada). Images were obtained through a parasternal short-axis

view with Mmode ultrasound at the level of the papillary muscle and midway between the papillary muscle and the apex. Ejection fractions were computed with the Vevo Lab 3.1.0 analysis software package. All analyses were performed by a single investigator blinded to the treatment assignment.

Whole mount immunofluorescence of neonatal hearts—Neonatal whole hearts were dissected in phosphate buffer saline (PBS), immediately fixed in 4% paraformaldehyde (PFA) at 4°C for 1 hour, followed by two 15-minutes washes with PBS at 4°C. The hearts were then incubated in primary antibodies prepared in at least 5 volumes of PBS containing 0.5% Triton (0.5% PBT) for 6 hours at room temperature (RT) followed by incubating them at 4°C overnight. The hearts were then washed in 20 volumes of 0.5% PBT for 6 hours with a change in wash buffer every hour at RT followed by a wash overnight at 4°C. The hearts were then incubated in 1:250 dilution of secondary antibodies prepared in 5 volumes of 0.5% PBT for 2 hours at RT followed by overnight at 4°C. The hearts were then washed in 20 volumes of 0.5% PBT for 6 consecutive days; for 6 hours at RT followed by overnight at 4°C each day. All steps were performed with gentle but continuous shaking. The hearts were finally cleared with 2 volumes of Vectashield (Vector; Cat: H-1000) for 2 hours at RT after which they were imaged immediately or stored in −20°C. Steps involving antibody or Vectashield incubations were performed in 1.5ml-2ml tubes and washes were performed in 50ml tubes.

Immunofluorescence on paraffin sections—Neonatal or adult hearts were fixed for 48 hours at 4°C, washed with PBS, dehydrated, paraffin embedded, and sectioned at 10μm. Four sections per heart were chosen at the low-papillary level and subjected to immunofluorescent staining. During the staining process, the hearts were dewaxed and rehydrated followed by antigen retrieval in preheated Sodium Citrate solution (pH= 6). The slides were then cooled down on ice and permeabilized using 0.5% PBT for 15 minutes at room temperature with agitation. Next, slides were washed with 1X PBS, placed in humidified chamber and blocked (with 5% Donkey serum, 0.3% Tween-20, 20mM $MgCl_2$ in 1X PBS) for 1 hour at room temperature. This step was followed by incubation of slides in primary antibodies diluted in above mentioned blocking solution over night at 4°C. The following day, slides were washed in 1X PBS, placed in humidified chamber and incubated in secondary antibodies (diluted in 5% BSA in 1X PBS) for 1 hour at room temperature. Next, slides were washed in 1X PBS, stained with DAPI for 15 minutes at room temperature, washed again with 1X PBS and mounted in Fluromount G (Southern Biotech; Cat: 0100-01) prior to confocal imaging.

Immunofluorescence on cryosections—Neonatal or adult hearts were fixed in 4% PFA for 1 hour at 4°C, washed in 1X PBS and incubated in 30% sucrose solution at 4°C over night. The following day, excessive sucrose was removed, hearts were embedded in OCT (Optical Cutting Temperature Compound, Fischer Health Care, Catalog: 4585), snap frozen on dry ice and stored in −80°C. 10μm cryosections were then prepared and stored at −80°C. To immunostain, tissue sections were thawed at room temperature for 15 minutes followed by two consecutive washes in 0.5% PBT and incubated in primary antibodies (made in 0.5% PBT) at 4°C over night. Next, the slides were washed in 0.5% PBT, and

incubated in secondary antibodies (made in 0.5% PBT) for 3 hours at room temperature followed by washes in 0.5% PBT. Cryosections were then mounted in Vectashield prior to confocal imaging.

Immunofluorescence on human-tissue sections—Tissue collection and examination was approved for use in research by the Stanford University Institutional Review Board. Myocardium was dissected from diseased human hearts that were explanted at the time of cardiac transplantation. Hearts were arrested with antegrade cold cardioplegia, surgically explanted, and transported in sterile saline and ice. Tissue was fixed in 4% Paraformaldehyde for one hour, washed in PBS, and snap froze in OCT. Tissue sections were washed in PBT, incubated in primary antibodies overnight at 4°C, washed again, and incubated in secondary antibodies at room temperature for 3 hours, followed by washes with PBT. Stained sections were mounted in Vectashield and imaged using an inverted Zeiss LSM-700 confocal microscope.

Masson's Trichrome staining—Hearts explanted 28 days (at P30) after surgery were fixed for 48 hours at 4°C, dehydrated, paraffin embedded, and sectioned at 10μm. One section per heart was chosen at the low-papillary level and stained with Masson's trichrome (Sigma-Aldrich; Cat: HT15–1KT). During the staining process, paraffin on the tissue sections was dissolved using xylene, the tissue was rehydrated with ethanol and fixed in Bouin's solution (not provided by the kit) for 15 minutes at RT followed by washes with running tap water for 2 minutes. The tissue sections were then incubated in Scarlet-Acid Fucshin for 15 mins, followed by phosphotungstic/phosphomolybdic acid solution acid as described in the manufacturer's manual. Next, the sections were stained in Aniline Blue for 15 minutes at RT followed by 2 minutes wash with running tap water. The sections were then incubated in 1% acetic acid solution (not provided by the kit) for 5 minutes at RT followed by washes with tap water for 2 minutes, dehydration and mounting in Cytoseal (Thermo Scientific; Cat: 8310-16). The slides were then imaged using an EVOS SL Core Imaging System (AMG; Cat: AMEX-1000) and processed using Adobe photoshop.

Confocal imaging of neonatal hearts—Whole neonatal hearts were flattened between a 1.5 mm thick microscope cover slip (Fisherbrand; Cat: 22266858) and a double concave microscope slide (Sail brand; Cat: 7104) with their anterior walls (watershed regions) facing the coverslip. The hearts were then imaged using inverted Zeiss LSM-700 confocal microscope. Whole hearts were scanned using 5X, 10X, 20X or 40X objectives. Digital images of multiple z-stacks for each scanned area were captured with Zeiss Zen software and stitched together using Adobe photoshop software.

Confocal imaging of adult hearts—Post-dissection, adult hearts were cleared with 2 volumes of Vectashield for 2 days at RT after which they were imaged immediately or stored in −20°C. Images of whole transgenic adult hearts were obtained with a Zeiss stereomicroscope (SteREO Discovery.V20). To image the watershed region, anterior wall of the adult hearts was sliced out and flattened onto concave slides as described above for neonate hearts. The anterior walls of adult hearts were imaged using an inverted Zeiss LSM-700 confocal microscope. Multiple images (from several comparable z-stacks) were

stitched together using “Grid/collection stitching” plugin from Image J at its default settings (sequential stitching with regression threshold at 0.3; Maximum average displacement threshold at 2.5; absolute displacement threshold at 3.5; Frame range at 1 and Linear blending to merge the images) (Preibisch et al., 2009; Zudaire et al., 2011).

Neonatal exposure to acute hypoxia—*Cxcl12-DsRed* transgenic pups were moved to oxygen control in vivo cabinets (from Biospherix) at P1, along with their nursing mother with access to food and water ad libitum. The air in the chamber was regulated by a mixture of room air and nitrogen while the oxygen levels were monitored by an oxygen analyzer (Servomex, Sugar Land, TX) and the temperature was maintained at 22-24°C. Excess CO_2 was removed by soda lime granules. An oxygen level of 10% was maintained in these hypoxic chambers for 4 days. Additional *Cxcl12-DsRed* transgenic litters were housed in normal oxygen levels to serve as normoxic control animals. *Cxcl12-Dsred* neonatal hearts were harvested at P4, fixed and analyzed after exposure to either hypoxia or normoxia for 4 days.

Foster-pup assay—*Cx40CreER; Rosa26*^{Tdtomato} P3 pups, previously unexposed to Tamoxifen, were transferred to and nursed by Tamoxifen injected (at P0) foster mother for 1 day (P2 through P3). These P3 transgenic pups were then sacrificed and hearts were analyzed for presence of any Tamoxifen induced *Cx40CreER*-labeled coronary artery cells.

Antibodies—Anti-CX40 (1:500; Alpha Diagnostics Int. Inc.; Cat: CX40-A), αSMA-FITC (1:300; Sigma; Cat: F3777), anti-ERG (1:500; Abcam; Cat: ab92513), CXCR4 (1:125; BD Pharminogen; Cat: 551852 and 1:300; abcam; Cat: 124824), Anti-PH3 (1:500; Millipore; Cat: 06-570), Anti-Myomesin (1:500; DSHB; B4-C), Anti-WGA (1:100, Invitrogen, Cat: W32466), Anti-ENDOMUCIN (1:300, Invitrogen, Cat: 14-5851-82), Anti-VEGFR2 (1:125, R&D Systems, Cat: AF644). Secondary reagents were Alexa fluor-conjugated antibodies (405, 488, 555, 633) from Life Technologies used at 1:250 dilutions.

QUANTIFICATION AND STATISTICAL ANALYSIS

Graphs represent mean values obtained from multiple experiments and error bars represent standard deviation. Unpaired student’s t-test was used to compare groups within an experiment and the level of significance were assigned to statistics in accordance to their p-values (0.05 flagged as *, 0.01 flagged as **, less than 0.001 flagged as ***, less than 0.0001 flagged as ****). All graphs were generated using GraphPad Prism software. Error bars represent ± standard deviation.

Collateral number and width—Number of lineage traced or CX40 immunostained collaterals were measured using Zeiss Zen image processing software from images obtained with a 10X objective.

Lineage cells in collaterals and artery tips—The extent of lineage cell coverage of collateral arteries was measured using images taken with 40X objective. Maximum projections of multiple z-stacks were created, stitched with Adobe photoshop and further analyzed using ImageJ software. Using selection tool in Image J, the entire area of the

collateral artery was manually traced (based on CX40 immunostain) and fluorescence intensity of lineage cells (red fluorescence) was measured. Measurements for percent area coverage of the red fluorescence (from multiple collaterals observed in the same heart and several other hearts) were then compiled to generate the graph.

Single artery cells within capillary EC layer—To determine the location of single artery cells in watershed areas with respect to capillary EC layer, confocal images taken with 40X objective of neonatal injured hearts (as shown in Figure 4H) were analyzed. Using Zeiss image processing software, artery cells that were both sharing eGFP^{+} cell junctions with capillary ECs and adjacent to the lumen as assessed by Lectin were counted as part of the capillary EC layer. Artery cells extending cell processes across capillaries into avascular regions of the watershed area were counted to be outside of the capillary EC layer.

Lectin re-perfusion—To quantify Lectin re-perfusion into the infarct area, confocal images taken with 10X objective of Lectin perfused P2 or P7 injured hearts were analyzed 4 days post-MI. Using Zeiss image processing software, mean fluorescence intensity (MFI) of Lectin was calculated from 4 non-infarct healthy regions and 4 infarct areas below the stitch for each heart injured at P2 or P7. MFI was measured from equivalent areas across all regions and hearts. For each heart, the 4 MFI measurements obtained from mal-perfused infarct areas below the stitch were plotted relative to average of MFIs obtained from healthy well-perfused areas for that same heart.

Artery cell migration—To quantify artery cell migration in injured neonatal hearts, confocal images taken with a 20X objective were used and the shortest distance between single artery cells closest to the ligated left coronary artery branches and those closest to the right coronary artery branches were measured using Zeiss image processing software.

Fibrotic scar area—To quantify scar area, serial tissue sections stained for Masson's Trichrome were used. Area of fibrotic scar (stained in blue, as shown in Figure S6E) and the entire left ventricle (stained in pink) were measured using ImageJ software for 4 comparable ventricular levels across all hearts and genotypes. The total relative scar area with respect to the total ventricular area, for each heart was plotted.

LCA width—The width of main left coronary artery was measured from confocal images taken at 10X magnification in whole mount preparations of neonatal hearts. Left coronary arteries were identified by CX40-immunostaining as shown in Figure S6B.

***Cx40CreER* or *ApjCreER* recombination—**All quantifications were performed using confocal images taken at 20X magnification in whole mount preparations of P3 neonatal hearts (Tamoxifen induction at P0). Arteries were identified based on CX40 immunostaining and capillaries based on co-staining for VEGFR2 and ENDOMUCIN. Maximum projections of multiple z-stacks were created and analyzed using ImageJ software. Using selection tool in Image J, the entire area of CX40^{+} large arteries were manually traced and percent area coverage of *Cx40CreER* or *ApjCreER* labeled cells (red fluorescence) were measured. Similarly, percent area coverage of *Cx40CreER* or *ApjCreER* labeled cells (red fluorescence) was measured in fields of view containing VEGFR2^{+} ENDOMUCIN^{+}

capillaries. Measurements for percent area coverage of the red fluorescence were taken from multiple arteries and fields of view containing capillaries in the same heart and several other hearts and compiled to generate the graph. Graph shown in Figure S1E is from n=32 arteries, n=23 fields of view with capillaries. Graph shown in Figure S3A is from n=25 arteries, n=21 fields of view with capillaries.

***Cx40CreER* labeling in foster pup experiment—**All quantifications were performed using confocal images taken with 20X objective, same gain and offset. Arteries were identified based on SMA-FITC immunostaining. Maximum projections of multiple z-stacks were created and analyzed using ImageJ software. Using selection tool in Image J, the entire area of SMA-FITC$^+$ large arteries were manually traced, and fluorescence mean intensity of *Cx40CreER* labeled cells (red fluorescence) were measured. Such measurements from multiple SMA-FITC$^+$ arteries and several hearts were then utilized to generate a graph.

Arteries and microvasculature post-MI—Percent area coverage of *Cx40CreER*-lineage labeled wildtype or *Cxcr4* depleted arteries were measured in whole heart images obtained by stitching several digital images of areas scanned with 5X objective (as shown in Figure 1C, D). Using ImageJ image processing software, these whole heart images were subjected to threshold to remove background and highlight arteries. Next, percent area coverage of *Cx40CreER* lineage labeled arteries were measured in the ischemic zone (below the stitch), watershed area and remote zone (away from injury). Measurements from several such hearts were compiled and a graph was generated. Graph shown in Figure S2F is compiled from n=5 control hearts (5 fields of view from ischemic zone, 16 fields of view from watershed area and 9 fields of view from remote zone), n=7 MI hearts (7 fields of view from ischemic zone, 12 fields of view from watershed area and 19 fields of view from remote zone) and n=5 $Cxcr4^{fl/fl}$; *Cx40CreER* hearts (19 fields of view from ischemic zone, 27 fields of view from watershed area and 21 fields of view from remote zone).

Cx40CreER; Rosa26^{Tdtomato}*; Tie2::eGFP;;Claudin5* transgenics were used to measure the changes in microvasculature (capillaries/veins/lymphatics) post-MI. Images of whole hearts were obtained and processed as mentioned above. All mages were taken with the same gain and offset. Using ImageJ software, percent area coverage of eGFP labeled microvasculature was measured in ischemic zone, watershed zone and remote zone in whole hearts and measurements from multiple hearts were compiled to generate a graph. Exclusion of Tdtomato$^+$ vessels ensured quantification of microvasculature and not arteries. Graph shown in Figure S2G is compiled from n=3 control hearts (20 fields of view from ischemic zone, 20 fields of view from watershed zone and 16 fields of view from remote zone) and n=3 MI hearts (21 fields of view from ischemic zone, 18 fields of view from watershed zone and 27 fields of view from remote zone).

EC proliferation—4 days post-MI *Cx40CreER; Rosa26*^{TdTomato} injured hearts were injected with 30μl of 10mM EdU (prepared in DMSO) for 30 minutes prior to immunostaining for EdU and ERG as mentioned earlier. EdU staining was performed with Click-iT staining kit provided by Invitrogen (Cat: C10337). Hearts were then subjected to whole mount confocal imaging and EdU$^+$ ECs were quantified in several ERG$^+$ TdTomato$^+$ artery tips, collateral arteries, single artery cells and fields of view containing (TdTomato$^-$

ERG$^+$) capillaries. Graph was compiled from n=17 control artery tips, 27 artery tips from MI hearts, 44 fields of view with control capillary cells, 55 fields of view with capillary cells from MI hearts, 151 single artery-derived single cells and 8 collateral arteries.

Cardiomyocyte proliferation—Hearts from *Cxcl12$^{fl/fl}$; Cdh5CreER* and *Cxcr4$^{fl/fl}$; Cx40CreER* knockouts and their littermate controls were harvested 7 days post-MI (MI at P2), fixed in 4% PFA for 48 hours at 4°C, washed, dehydrated, embedded in paraffin and sectioned at 10μm. Two sections per heart were chosen at the low-papillary level and immunostained for Myomesin, WGA, PH3 and DAPI as mentioned above and images were obtained at 20X (Octavar-1). DAPI$^+$ PH3$^+$ Myomesin$^+$ cells enclosed by Wheat Germ Agglutinin (WGA) were quantified from 2 adjacent tissue sections. 4-8 fields of view were collected for ischemic, border and remote zones from these two sections. Measurements from 5 control and 5-7 knockout animals (for each genotype) were then compiled to generate a graph.

Supplementary Material

Refer to Web version on PubMed Central for supplementary material.

Acknowledgments:

We thank Dr. Lucile Miquerol for the *Cx40CreER* mouse line and Dr. Ralf Adams for the *Cdh5CreER* mouse line. K.R. is supported by the NIH (RO1-HL128503) and the New York Stem Cell Foundation (Robertson Investigator). Y.J.W. is supported by NIH (1R01HL089315). A.B.G. is supported by American Heart Association (14POST20380744). H.W. is supported by American Heart Association (18POST33990223). M.J.P is supported by American Heart Association (17POST33410497). D.A. is funded by the NIH (R01MH112849 and R01NS107344) and The Foundation Leducq (15CVD-02). We thank all members of the Red-Horse and Woo laboratories for their constructive feedback during the preparation of manuscript.

References

Abbott JD, Huang Y, Liu D, Hickey R, Krause DS, and Giordano FJ (2004). Stromal cell-derived factor-1alpha plays a critical role in stem cell recruitment to the heart after myocardial infarction but is not sufficient to induce homing in the absence of injury. Circulation 110, 3300–3305. [PubMed: 15533866]

Askari AT, Unzek S, Popovic ZB, Goldman CK, Forudi F, Kiedrowski M, Rovner A, Ellis SG, Thomas JD, DiCorleto PE, et al. (2003). Effect of stromal-cell-derived factor 1 on stem-cell homing and tissue regeneration in ischaemic cardiomyopathy. Lancet 362, 697–703. [PubMed: 12957092]

Aurora AB, Porrello ER, Tan W, Mahmoud AI, Hill JA, Bassel-Duby R, Sadek HA, and Olson EN (2014). Macrophages are required for neonatal heart regeneration. J. Clin. Invest 124, 1382–1392. [PubMed: 24569380]

Bassat E, Mutlak YE, Genzelinakh A, Shadrin IY, Baruch Umansky K, Yifa O, Kain D, Rajchman D, Leach J, Riabov Bassat D, et al. (2017). The extracellular matrix protein agrin promotes heart regeneration in mice. Nature 547, 179–184. [PubMed: 28581497]

Baxter R, Hastings N, Law A, and Glass EJ. (2008). CXCL12 gene expression is upregulated by hypoxia and growth arrest but not by inflammatory cytokines in rheumatoid synovial fibroblasts. Anim. Genet 39, 561–563. [PubMed: 18637877]

Cavallero S, Shen H, Yi C, Lien CL, Kumar SR, and Sucov HM (2015). CXCL12 Signaling is Essential for Maturation of the Ventricular Coronary Endothelial Plexus and Establishment of Functional Coronary Circulation. Dev. Cell 33, 469–477. [PubMed: 26017771]

Ceradini DJ, Kulkarni AR, Callaghan MJ, Tepper OM, Bastidas N, Kleinman ME, Capla JM, Galiano RD, Levine JP, and Gurtner GC (2004). Progenitor cell trafficking is regulated by hypoxic gradients through HIF-1 induction of SDF-1. Nat. Med 10, 858–864. [PubMed: 15235597]

Chang AH, Raftrey BC, D'Amato G, Surya VN, Poduri A, Chen HI, Goldstone AB, Woo J, Fuller GG, Dunn AR, et al. (2017). DACH1 stimulates shear stress-guided EC migration and coronary artery growth through the CXCL12-CXCR4 signaling axis. Genes Dev. 31, 1308–1324. [PubMed: 28779009]

Chen HI, Sharma B, Akerberg BN, Numi HJ, Kivela R, Saharinen P, Aghajanian H, McKay AS, Bogard PE, and Chang AH (2014). The sinus venosus contributes to coronary vasculature through VEGFC-stimulated angiogenesis. Development 141, 4500–4512. [PubMed: 25377552]

Dong F, Harvey J, Finan A, Weber K, Agarwal U, and Penn MS (2012). Myocardial CXCR4 expression is required for mesenchymal stem cell mediated repair following acute myocardial infarction. Circulation 126, 314–324. [PubMed: 22685115]

Döring Y, Pawig L, Weber C, and Noels H (2014). The CXCL12/CXCR4chemokine ligand/receptor axis in cardiovascular disease. Front. Physiol. 5 6.

Faber JE, Chilian WM, Deindl E, Van Royen N, and Simons M (2014). A brief etymology of the collateral circulation. Arterioscler. Thromb. Vasc. Biol 34, 1854–1859. [PubMed: 25012127]

Gabhann F. Mac, and Peirce SM (2010). Collateral capillary arterialization following arteriolar ligation in murine skeletal muscle. Microcirculation 17, 333–347. [PubMed: 20618691]

Ghasemzadeh N, Hritani AW, De Staercke C, Eapen DJ, Veledar E, Al Kassem H, Khayata M, Zafari AM, Sperling L, Hooper C, et al. (2015). Plasma stromal cell-derived factor 1α/CXCL12 level predicts long-term adverse cardiovascular outcomes in patients with coronary artery disease. Atherosclerosis 238, 113–118. [PubMed: 25461737]

Go AS, Mozaffarian D, Roger VL, Benjamin EJ, Berry JD, Blaha MJ, Dai S, Ford ES, Fox CS, Franco S, et al. (2014). Heart disease and stroke statistics--2014 update: a report from the American Heart Association. Circulation 129, e28–e292. [PubMed: 24352519]

Goldstone AB, Burnett CE, Cohen JE, Paulsen MJ, Eskandari A, Edwards BE, Ingason AB, Steele AN, Patel JB, Macarthur JW, et al. (2018). SDF 1-alpha Attenuates Myocardial Injury Without Altering the Direct Contribution of Circulating Cells.

Habib GB, Heibig J, Forman SA, Brown BG, Roberts R, Terrin ML, and Bolli R (1991). Influence of coronary collateral vessels on myocardial infarct size in humans. Results of phase I thrombolysis in myocardial infarction (TIMI) trial. The TIMI Investigators. Circulation 83, 739–746. [PubMed: 1900223]

Hagensen MK, Abe AS, Falk E, and Wang T (2008). Physiological importance of the coronary arterial blood supply to the rattlesnake heart. J. Exp. Biol 211, 3588–3593. [PubMed: 18978223]

Hara R, McGinley J, Briggs C, Baker R, and Sangeux M (2016). Predicting the location of the hip joint centres, impact of age group and sex. Sci. Rep 6, 37707. [PubMed: 27883044]

Harrison MRM, Bussmann J, Huang Y, Zhao L, Osorio A, Burns CG, Burns CE, Sucov HM, Siekmann AF, and Lien CL (2015). Chemokine-Guided Angiogenesis Directs Coronary Vasculature Formation in Zebrafish. Dev. Cell 33, 442–454. [PubMed: 26017769]

Haubner BJ, Adamowicz-Brice M, Khadayate S, Tiefenthaler V, Metzler B, Aitman T, and Penninger JM (2012). Complete cardiac regeneration in a mouse model of myocardial infarction. Aging (Albany NY) 4, 966–977. [PubMed: 23425860]

Haubner BJ, Schuetz T, and Penninger JM (2016). A reproducible protocol for neonatal ischemic injury and cardiac regeneration in neonatal mice. Basic Res. Cardiol. Ill, 1–10.

He L, Liu Q, Hu T, Huang X, Zhang H, Tian X, Yan Y, Wang L, Huang Y, Miquerol L, et al. (2016). Genetic lineage tracing discloses arteriogenesis as the main mechanism for collateral growth in the mouse heart. Cardiovasc. Res 109, 419–430. [PubMed: 26768261]

He L, Huang X, Kanisicak O, Li Y, Wang Y, Li Y, Pu W, Liu Q, Zhang H, Tian X, et al. (2017). Preexisting ECs mediate cardiac neovascularization after injury. J. Clin. Invest 127, 2968–2981. [PubMed: 28650345]

Helfant RH, Vokonas PS, and Gorlin R (1971). Functional importance of the human coronary collateral circulation. N. Engl. J. Med 284, 1277–1281. [PubMed: 5576437]

Hiesinger W, Perez-Aguilar JM, Atluri P, Marotta NA, Frederick JR, Fitzpatrick JR, McCormick RC, Muenzer JR, Yang EC, Levit RD, et al. (2011). Computational protein design to reengineer stromal cell-derived factor-1α generates an effective and translatable angiogenic polypeptide analog. Circulation 124, S18–26. [PubMed: 21911811]

Hitchon C, Wong K, Ma G, Reed J, Lyttle D, and El-Gabalawy H (2002). Hypoxia-induced production of stromal cell-derived factor 1 (CXCL12) and vascular endothelial growth factor by synovial fibroblasts. Arthritis Rheum. 46, 2587–2597. [PubMed: 12384916]

Hu X, Dai S, Wu W-J, Tan W, Zhu X, Mu J, Guo Y, Bolli R, and Rokosh G (2007). Stromal cell derived factor-1 alpha confers protection against myocardial ischemia/reperfusion injury: role of the cardiac stromal cell derived factor-1 alpha CXCR4 axis. Circulation 116, 654–663. [PubMed: 17646584]

Ingason AB, Goldstone AB, Paulsen MJ, Thakore A, Truong V, Edwards BB, Eskandari A, Bollig T, Steele AN, and Woo YJ (2017). Angiogenesis Precedes Cardiomyocyte Migration in Regenerating Mammalian Hearts. J. Thorac. Cardiovasc. Surg 155, 1118–1127.e1. [PubMed: 29452461]

Ivins S, Chappell J, Vernay B, Suntharalingham J, Martineau A, Mohun TJ, and Scambler PJ (2015). The CXCL12/CXCR4 Axis Plays a Critical Role in Coronary Artery Development. Dev. Cell 33, 455–468. [PubMed: 26017770]

Kiechl S, Laxton RC, Xiao Q, Hernesniemi JA, Raitakari OT, Kähönen M, Mayosi BM, Jula A, Moilanen L, Willeit J, et al. (2010). Coronary artery disease-related genetic variant on chromosome 10q11 is associated with carotid intima-media thickness and atherosclerosis. Arterioscler. Thromb. Vasc. Biol 30, 2678–2683. [PubMed: 20847302]

Kim EK, Choi J-H, Song Y. Bin, Hahn J-Y, Chang S-A, Park S-J, Lee S-C, Choi S-H, Choe YH, Park SW, et al. (2016). A protective role of early collateral blood flow in patients with ST-segment elevation myocardial infarction. Am. Heart J 171, 56–63. [PubMed: 26699601]

Knowland D, Arac A, Sekiguchi KJ, Hsu M, Lutz SE, Perrino J, Steinberg GK, Barres BA, Nimmerjahn A, and Agalliu D (2014). Stepwise Recruitment of Transcellular and Paracellular Pathways Underlies Blood-Brain Barrier Breakdown in Stroke. Neuron 82, 603–617. [PubMed: 24746419]

Kryczek I, Lange A, Mottram P, Alvarez X, Cheng P, Hogan M, Moons L, Wei S, Zou L, Machelon V, et al. (2005). CXCL12 and vascular endothelial growth factor synergistically induce neonaniogenisis in human ovarian cancers. Cancer Res. 65, 465–472. [PubMed: 15695388]

Lavine KJ, Kovacs A, Weinheimer C, and Mann DL (2013). Repetitive myocardial ischemia promotes coronary growth in the adult mammalian heart. J. Am. Heart Assoc 2.

Lutz SE, Smith JR, Kim DH, Olson CVL, Ellefsen K, Bates JM, Gandhi SP, and Agalliu D (2017). Caveolin1 Is Required for Th1 Cell Infiltration, but Not Tight Junction Remodeling, at the Blood-Brain Barrier in Autoimmune Neuroinflammation. Cell Rep. 21, 2104–2117. [PubMed: 29166603]

Macarthur JW, Cohen JE, Mcgarvey JR, Shudo Y, Patel JB, Trubelja A, Fairman AS, Edwards BB, Hung G, Hiesinger W, et al. (2014). Preclinical evaluation of the engineered stem cell chemokine stromal cell-derived factor 1α analog in a translational ovine myocardial infarction model. Circ. Res 114, 650–659. [PubMed: 24366171]

Mahmoud A, Porrello E, and Kimura W (2014). Surgical models for cardiac regeneration in neonatal mice. Nat. Protoc 9, 305–311. [PubMed: 24434799]

Marin-Juez R, Marass M, Gauvrit S, Rossi A, Lai SL, Materna SC, Black BL, Stainier DY, and Sci USA (2016). Fast revascularization of the injured area is essential to support zebrafish heart regeneration. Proc Natl Acad 113, 11237–11242.

Mehta NN, Li M, William D, Khera AV, Derohannessian S, Qu L, Ferguson JF, McLaughlin C, Shaikh LH, Shah R, et al. (2011). The novel atherosclerosis locus at 10q11 regulates plasma CXCL12 levels. Eur. Heart J 32, 963–971. [PubMed: 21415067]

Mehta NN, Matthews GJ, Krishnamoorthy P, Shah R, McLaughlin C, Patel P, Budoff M, Chen J, Wolman M, Go A, et al. (2014). Higher plasma CXCL12 levels predict incident myocardial infarction and death in chronic kidney disease: Findings fromthe chronic renal insufficiency cohort study. Eur. Heart J 35.

Meier P, Lansky AJ, Fahy M, Xu K, White HD, Bertrand ME, Mehran R, and Stone GW (2014). The impact of the coronary collateral circulation on outcomes in patients with acute coronary syndromes: results from the ACUITY trial. Heart 100, 647–651. [PubMed: 24310521]

Meier RPH, Müller YD, Morel P, Gonelle-Gispert C, and Bühler LH (2013). Transplantation of mesenchymal stem cells for the treatment of liver diseases, is there enough evidence? Stem Cell Res. 11, 1348–1364. [PubMed: 24090934]

Miquerol L, Thireau J, Bideaux P, Sturny R, Richard S, and Kelly RG (2015). Endothelial plasticity drives arterial remodeling within The endocardium after myocardial infarction. Circ. Res 116, 1765–1771. [PubMed: 25834185]

Penn MS, Pastore J, Miller T, and Aras R (2012). SDF-1 in myocardial repair. Gene Ther. 19, 583–587. [PubMed: 22673496]

Porrello ER, Mahmoud AI, Simpson E, Hill JA, Richardson JA, Olson EN, and Sadek HA (2011). Transient regenerative potential of the neonatal mouse heart. Science (80-.). 331, 1078–1080.

Porrello ER, Mahmoud AI, Simpson E, Johnson BA, Grinsfelder D, Canseco D, Mammen PP, Rothermel BA, Olson EN, and Sadek HA (2013). Regulation of neonatal and adult mammalian heart regeneration by the miR-15 family. Proc. Natl. Acad. Sci 110, 187–192. [PubMed: 23248315]

Preibisch S, Saalfeld S, and Tomancak P (2009). Globally optimal stitching of tiled 3D microscopic image acquisitions. Bioinformatics 25, 1463–1465. [PubMed: 19346324]

Quaife-Ryan GA, Sim CB, Ziemann M, Kaspi A, Rafehi H, Ramialison M, El-Osta A, Hudson JE, and Porrello ER (2017). Multicellular transcriptional analysis of mammalian heart regeneration. Circulation 136, 1123–1139. [PubMed: 28733351]

Samani NJ, Erdmann J, Hall AS, Hengstenberg C, Mangino M, Mayer B, Dixon RJ, Meitinger T, Braund P, Wichmann H-E, et al. (2007). Genomewide Association Analysis of Coronary Artery Disease. N. Engl. J. Med 357, 443–453. [PubMed: 17634449]

Saxena A, Fish JE, White MD, Yu S, Smyth JWP, Shaw RM, DiMaio JM, and Srivastava D (2008). Stromal cell-derived factor-1alpha is cardioprotective after myocardial infarction. Circulation 117, 2224–2231. [PubMed: 18427137]

Schunkert H, König I, and Kathiresan S (2011). Large-scale association analyses identifies 13 new susceptibility loci for coronary artery disease. Nat. Genet 43, 333–338. [PubMed: 21378990]

Segers VFM, Tokunou T, Higgins LJ, MacGillivray C, Gannon J, and Lee RT (2007). Local delivery of protease-resistant stromal cell derived factor-1 for stem cell recruitment after myocardial infarction. Circulation 116, 1683–1692. [PubMed: 17875967]

Seiler C, Stoller M, Pitt B, and Meier P (2013). The human coronary collateral circulation: development and clinical importance. Eur. Heart J 34, 2674–2682. [PubMed: 23739241]

Simons M, and Eichmann A (2015). Molecular controls of arterial morphogenesis. Circ. Res 116, 1712–1724. [PubMed: 25953926]

Su T, Stanley G, Sinha R, D'Amato G, Das S, Rhee S, Chang AH, Poduri A, Raftrey B, Dinh TT, et al. (2018). Single-cell analysis of early progenitor cells that build coronary arteries. Nature 559, 356–362. [PubMed: 29973725]

Sundararaman S, Miller TJ, Pastore JM, Kiedrowski M, Aras R, and Penn MS (2011). Plasmid-based transient human stromal cell-derived factor-1 gene transfer improves cardiac function in chronic heart failure. Gene Ther. 18, 867–873. [PubMed: 21472007]

Tabatabai G, Frank B, Möhle R, Weller M, and Wick W (2006). Irradiation and hypoxia promote homing of haematopoietic progenitor cells towards gliomas by TGF-β-dependent HIF-1α-mediated induction of CXCL12. Brain 129, 2426–2435. [PubMed: 16835250]

Tang J, Zhang H, He L, Huang X, Li Y, Pu W, Yu W, Zhang L, Cai D, Lui KO, et al. (2018). Genetic Fate Mapping Defines the Vascular Potential of Endocardial Cells in the Adult Heart. Circ. Res CIRCRESAHA.117.312354.

Tzahor E, and Poss KD (2017). Cardiac regeneration strategies: Staying young at heart. Science 356, 1035–1039. [PubMed: 28596337]

Wang Y, Nakayama M, Pitulescu ME, Schmidt TS, Bochenek ML, Sakakibara A, Adams S, Davy A, Deutsch U, Lüthi U, et al. (2010). Ephrin-B2 controls VEGF-induced angiogenesis and lymphangiogenesis. Nature 465, 483–486. [PubMed: 20445537]

Wustmann K, Zbinden S, Windecker S, Meier B, and Seiler C (2003). Is there functional collateral flow during vascular occlusion in angiographically normal coronary arteries? Circulation 107, 2213–2220. [PubMed: 12707241]

Zhang H, and Faber JE (2015). De-novo collateral formation following acute myocardial infarction: Dependence on CCR2+bone marrow cells. J. Mol. Cell. Cardiol 87, 4–16. [PubMed: 26254180]

Zhao L, Borikova AL, Ben-Yair R, Guner-Ataman B, MacRae CA, Lee RT, Burns CG, and Burns CE (2014). Notch signaling regulates cardiomyocyte proliferation during zebrafish heart regeneration. Proc. Natl. Acad. Sci. U. S. A 111, 1403–1408. [PubMed: 24474765]

Ziff OJ, Bromage DI, Yellon DM, and Davidson SM (2018). Therapeutic strategies utilizing SDF-1α in ischaemic cardiomyopathy. Cardiovasc. Res 114, 358–367. [PubMed: 29040423]

Zimarino M, D'Andreamatteo M, Waksman R, Epstein SE, and De Caterina R (2014). The dynamics of the coronary collateral circulation. Nat. Rev. Cardiol 11, 191–197. [PubMed: 24395049]

Zudaire E, Gambardella L, Kurcz C, and Vermeren S (2011). A computational tool for quantitative analysis of vascular networks. PLoS One 6, 1–12.

- Artery endothelial cells (ECs) of neonatal hearts have a unique response to injury
- Injury stimulates artery cell migration and reassembly into collateral arteries
- CXCL12/CXCR4 signaling guides Artery Reassembly, facilitating heart regeneration
- Adult artery ECs can be induced to undergo Artery Reassembly with exogenous CXCL12

A neonatal regenerative pathway in that involves the migration of arterial endothelial cells to build collateral arteries that can provide blood flow under conditions of infarction or vascular occlusion has the potential to be harnessed for adult ischemic heart disease.

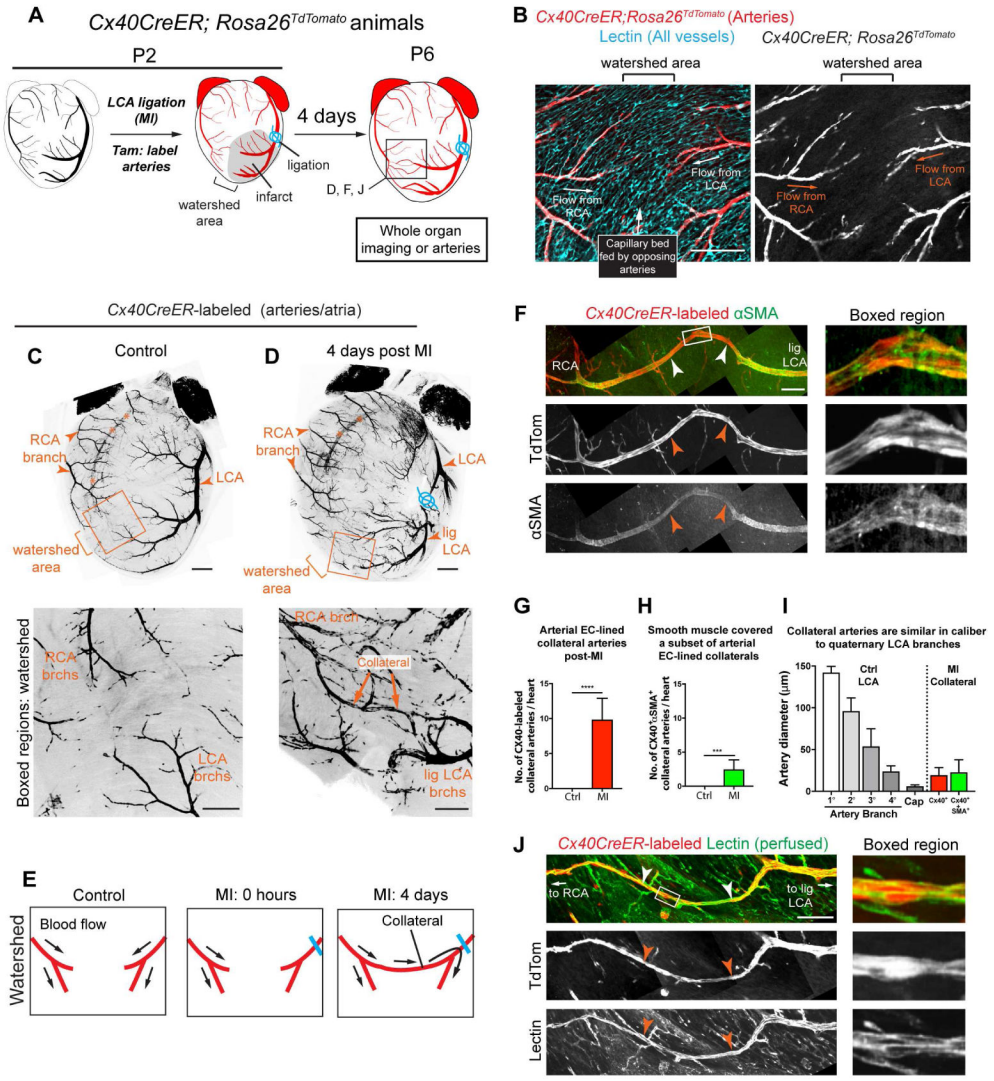

Figure 1. Extensive collateral artery formation in the neonatal mouse heart 4 days post MI. See also Figure S1 and S2.

(**A**) Experimental design where *Cx40CreER*-labeled arteries are red.(**B**) Confocal image of a watershed area from P2 control heart. Capillary bed (cyan) is fed by left (LCA) and right (RCA) coronary artery branches. (**C** and **D**) Confocal images (anterior views) of control (**C**) and myocardial infarction (MI) (**D**) hearts. Arterial ECs are black. MI induced collateral arteries that connect ligated (lig) branches (brchs) of LCA with RCA branches across the watershed area (boxed regions). Asterisks are RCA showing through from the posterior heart wall. (**E**) Schematic of how collateral arteries restore blood flow (arrows) to injured myocardium. Arteries, red; ligation, blue. (**F**) Some *Cx40CreER*-labeled collateral arteries contain smooth muscle. (**G** and **H**) Quantification of *Cx40CreER*-labeled (**G**) and smooth muscle covered (**H**) collateral arteries. Hearts: n=8 control, n=12 MI. (**I**) Collateral arteries were similar in diameter to quaternary (4°) branches . Arteries: N=24 $CX40^{+}$, n=9 αSMA^{+}. (**J**) Collateral arteries were perfused. Cap, capillaries; P, postnatal; Tam, Tamoxifen; EC,

endothelial cells; TdTom, TdTomato. Scale bars: **B**, 200μm; **C, D** low mag, 500μm; **C, D** boxed region, 200μm; **F** and **J**, 200μm. Error bars are st dev: ***, p≤0.001; ****, p≤0.0001.

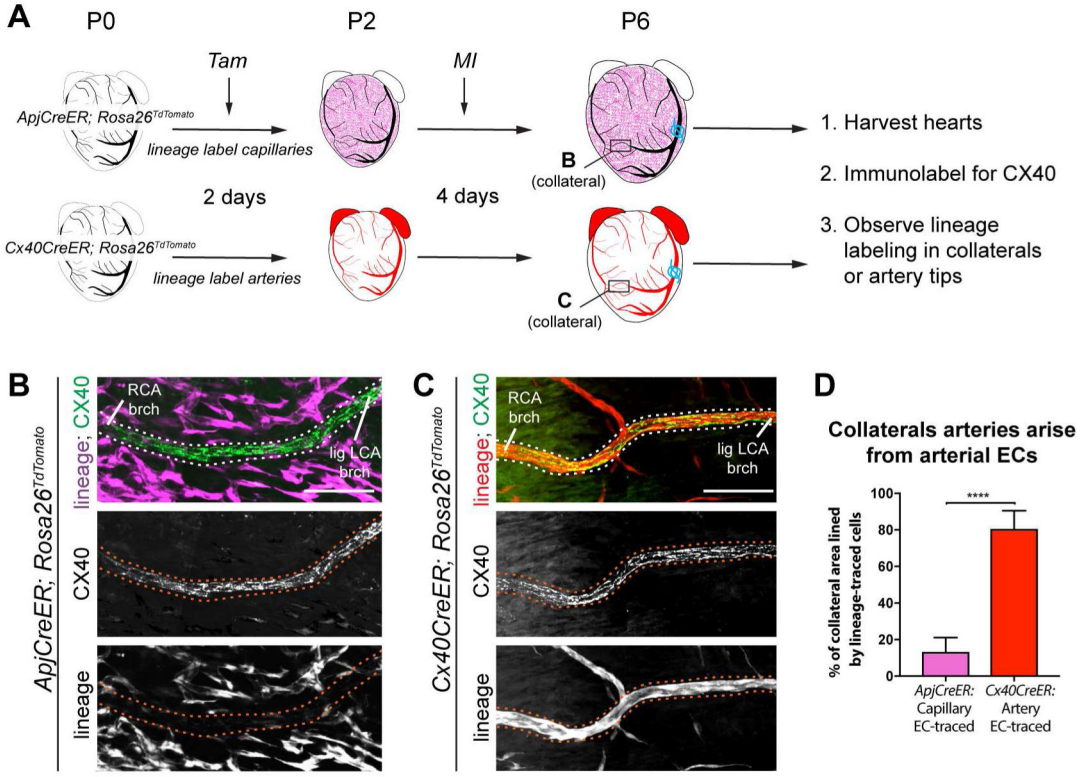

Figure 2. Collateral arteries are formed by arterial endothelial cells. See also Figure S3.

(**A**) Experimental design where non-labeled arteries are black and lineage-labeled capillaries or arteries are magenta or red, respectively. Boxes localize collateral arteries in **B** and **C.** (**B** and **C**) CX40^{+} collateral arteries (dotted lines) showed minimal *ApjCreER* lineage labeling from capillaries (**B**), but heavy lineage-labeling *Cx40CreER*$^{+}$ arteries (**C**). (**D**) Quantification of **B** and **C** (n=7 arteries each). Lig LCA, ligated left coronary artery; MI, myocardial infarction; RCA, right coronary artery; Tam, Tamoxifen; P, postnatal; EC, endothelial cells; brch, branch. Scale bars: 100μm. Error bars are st dev: ****, p≤0.0001.

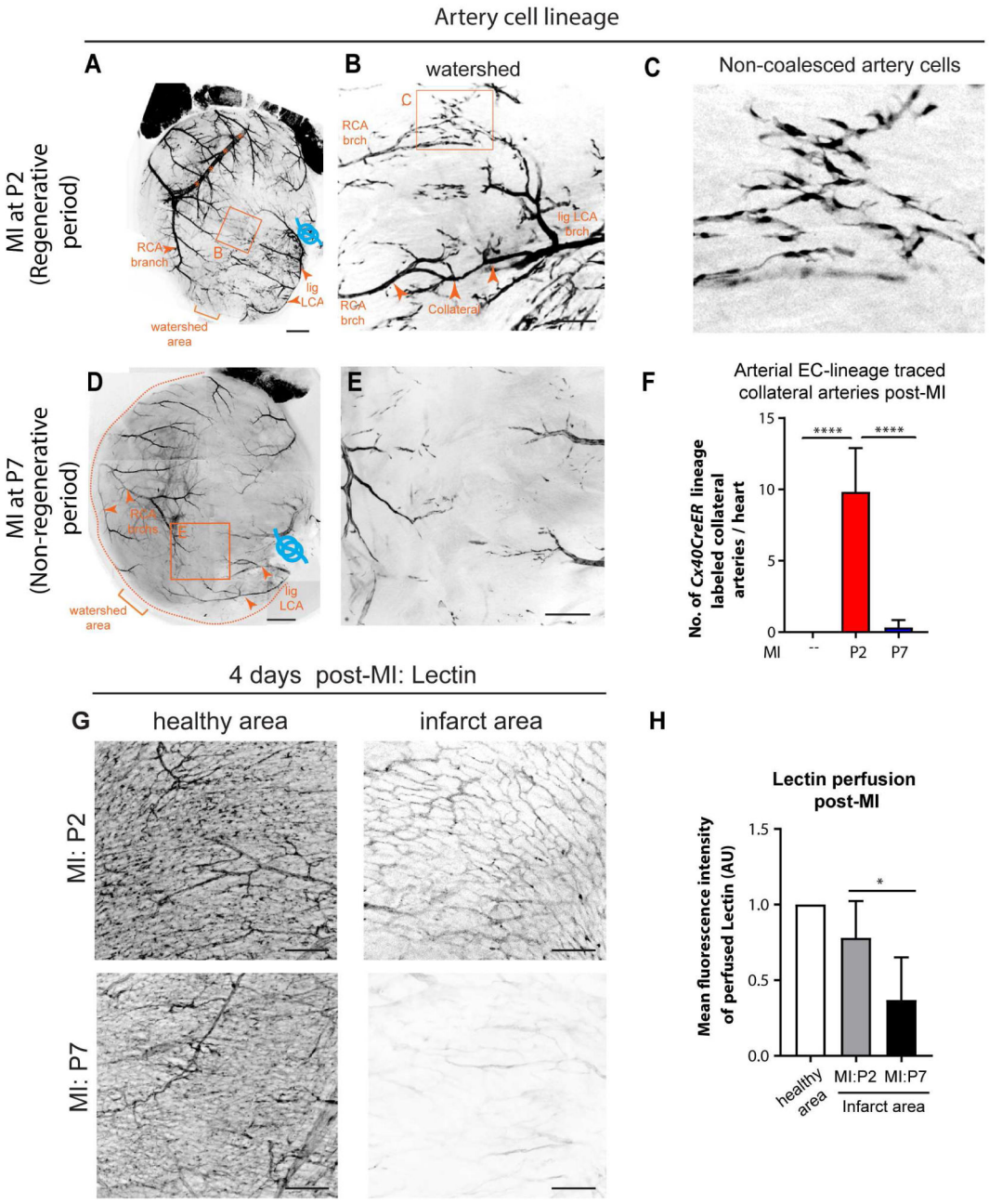

Figure 3: Artery-derived collateral development is restricted to the neonatal regenerative window.

(**A**) Anterior view of P6 *Cx40CreER; Rosa26*^{TdTomato} heart. Tamoxifen at P0, MI at P2, and harvested 4 days post-MI. Arteries are black, ligation in blue. Asterisks, right coronary artery (RCA) from posterior heart wall. (**B**) Boxed region from **A**. Arrowheads, collateral artery spanning watershed region. (**C**) Boxed region from **B** with non-coalesced arterial ECs in space between ligated left coronary artery (lig LCA) and non-ligated RCA branches. Pattern seen in n=8 hearts. (**D**) Anterior view of P11 *Cx40CreER; Rosa26*^{TdTomato}. Tamoxifen at P0, ligated at P7, and harvested 4 days post-MI. (**E**) Boxed region from **D**

reveal few lineage labeled artery cells in watershed and no collateral arteries. (**F**) Quantification at 4 days post-MI. Hearts: P2, n=12; P7, n=6. (**G**) Lectin perfusion in healthy and infarcted heart regions injured at P2 or P7, 4 days post-MI. (**H**) Quantification of mean fluorescence intensity. Hearts: P7, n=6, P2 n=6. Brch, branch; P, postnatal; EC, endothelial cells; MI, myocardial infarction. Scale bars: **A** and **D,** 500μm; **B** and **E**, 200 μm; **G**, 100μm. Error bars are st dev: *, $p \leq 0.05$; ****, $p \leq 0.0001$.

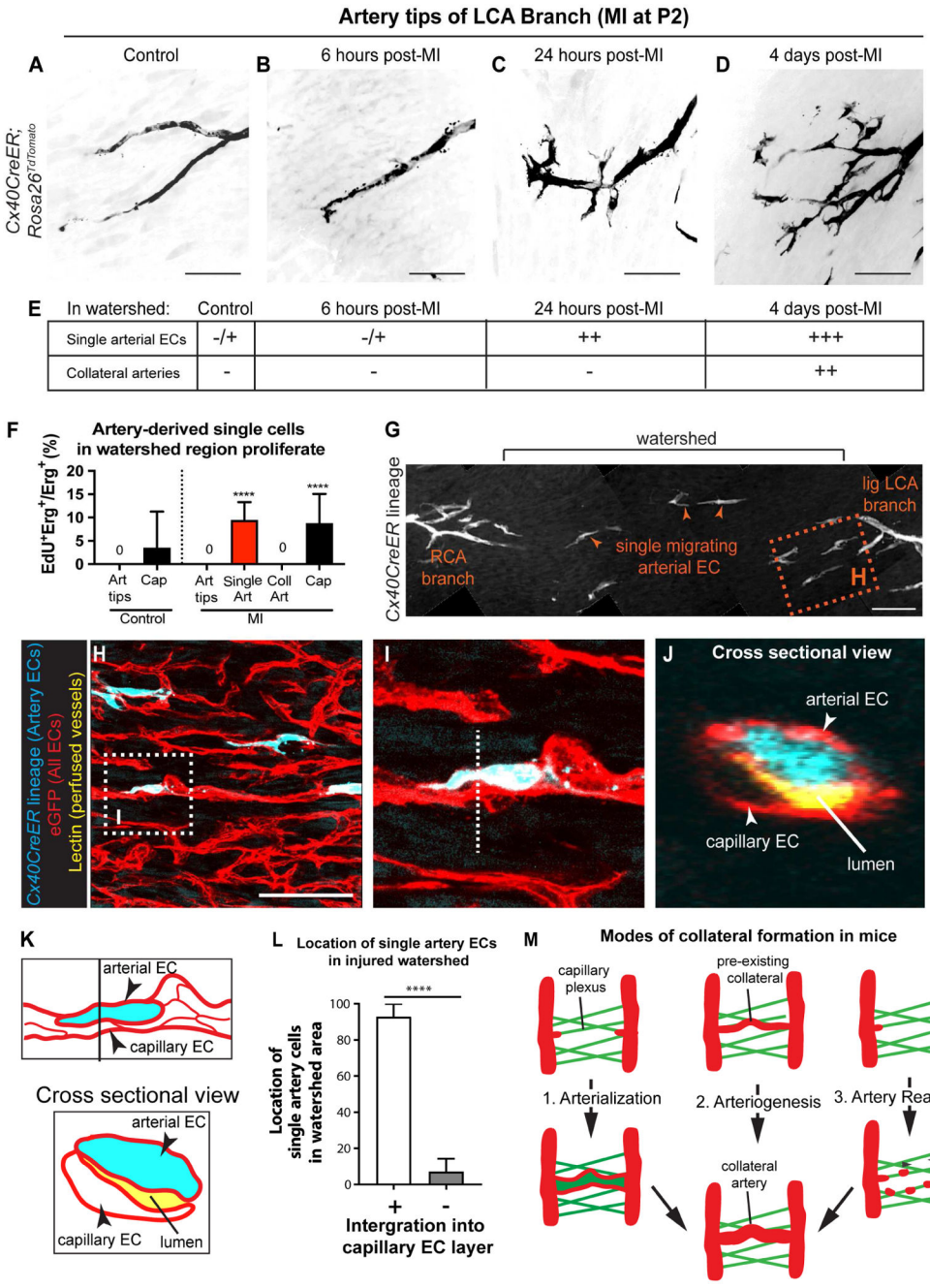

Figure 4. Migration of individual arterial ECs precedes the appearance of artery-derived collaterals. See also Figure S4.

(**A-D**) LCA tips from control or injured hearts. Arterial ECs appear mobilized within 24 hours. Tamoxifen injected at P0; MI at P2. Pattern seen in n=6 control and n=4 MI hearts each. (**E**) Table summarizing single arterial ECs in watersheds before collateral artery development. –, absent; −/+, very few; ++, many; +++, very many. (**F**) EdU incorporation indicates that artery cells in watershed proliferate. Hearts: n=2 control, n=3 MI. (**G-J**) *Cx40CreER; Rosa26*^{TdTomato}*; Tie2;:eGFP::Claudin5* hearts subjected to MI at P2 and Lectin perfused before isolation at P6. (**G**) Single artery cells (arrowheads) in watershed area 4

days post-MI. (**H**) Box in **G** showing arterial ECs (cyan) closely associated with capillaries (red). (**I**) Box in **H**. (**J**) Cross-section view (dotted line in **I).** Artery cell is adjacent to perfused Lectin (yellow), indicating it's within EC layer. (**K**) Schematic of **I** and **J**. EC (**L**) Quantification where single artery cells are within EC layer (n=5 hearts). (**M**) Schematic adding Artery Reassembly to the different modes of collateral artery formation. LCA, left coronary artery; MI, myocardial infarction; P, postnatal; Cap, capillary; Coll, collateral artery; Art, artery. Scale bars:100μm. Error bars are st dev: ****, p≤0.0001.

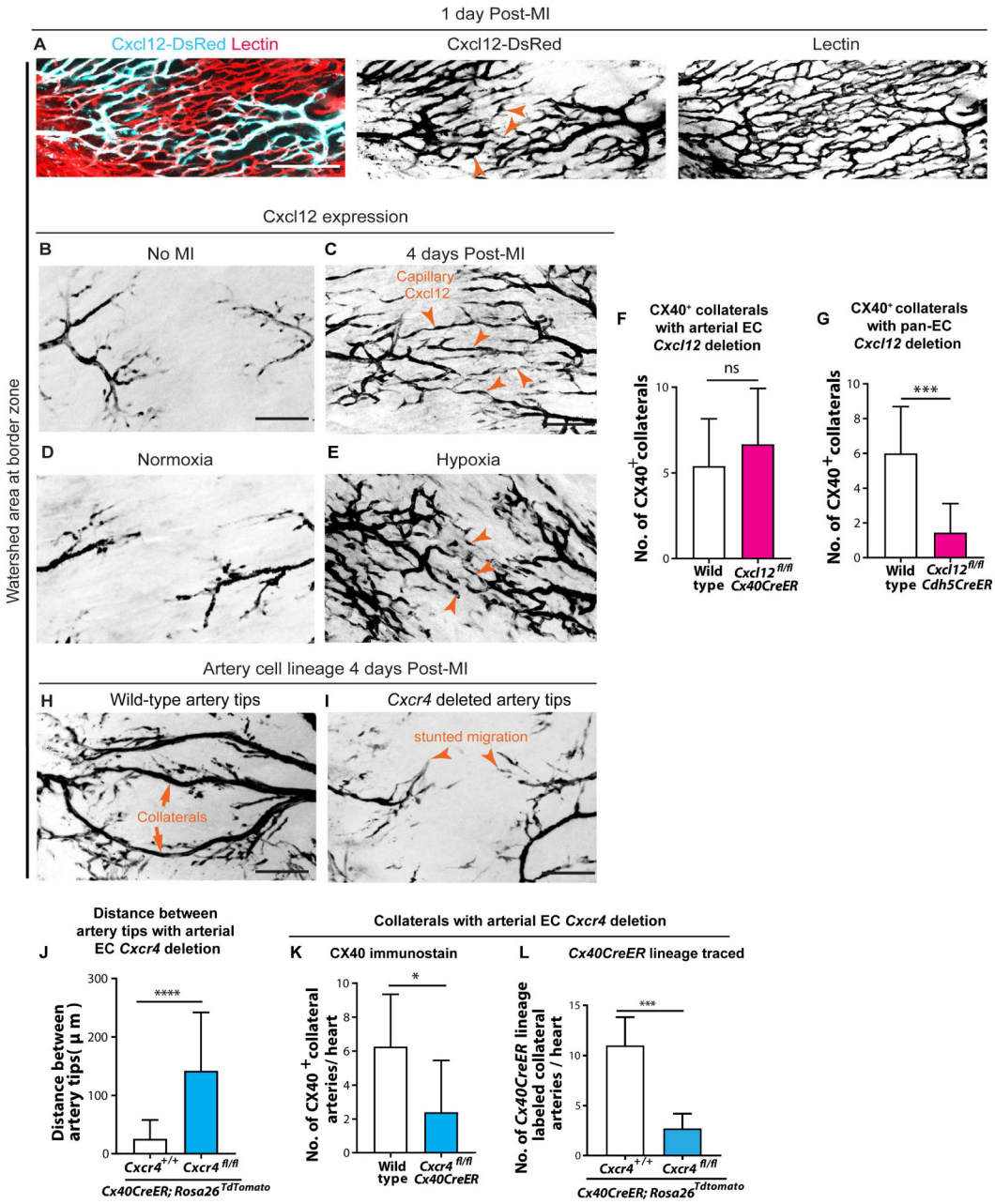

Figure 5. CXCR4 signaling guides arterial migration during collateral formation. See also Figure S5 and S6.

(**A**) *Cxcl12-DsRed* expression in watershed capillaries 1 day post-myocardial infarction (MI). Pattern seen in 4 hearts. (**B**-**E**) *Cxcl12-DsRed* in P6 hearts. *Cxcl12* is in artery tips in non-injured hearts (**B**), but is induced in capillary ECs in watershed upon MI (arrowheads, **C**). Pattern seen in n=4 control and n=6 MI hearts. In comparison to normoxic conditions (**D**), hypoxia expands *Cxcl12-DsRed* into capillary ECs (arrowheads, **E**). Pattern seen in n=4 normoxic hearts and n=13 hypoxic hearts. (**F** and **G**) CX40^{+} collaterals in injured P6 hearts following arterial *Cxcl12* deletion (**F**) (n=10 wild-type, n=6 knockout (KO) hearts) or pan-EC *Cxcl12* deletion (**G**) ECs (n=14 wild-type, n=9 KO hearts). (**H** and **I**) *Cx40CreER*-

lineage labeled artery cells and collaterals (**H**) in watershed are dramatically decreased with EC arterial *Cxcr4* deletion (**I**). (**J**-**L**) Number of single arterial ECs in watershed (**J**) (n=3 wild-type, n=4 KO hearts), $CX40^{+}$ collaterals (**K**) (n=2 wild-type, n=6 KO hearts), and *Cx40CreER* lineage-traced collaterals (**L**) (n=11 wild-type, n=5 KO hearts) is significantly reduced upon arterial deletion of *Cxcr4*. All deletions induced at P0; MIs at P2. lig, ligated; LCA, left coronary artery; RCA, right coronary artery; P, postnatal; EC, endothelial cell. Scale bars: 100μm. Error bars are st dev: *, p≤0.05; ***, p≤0.001, ****, p≤0.0001.

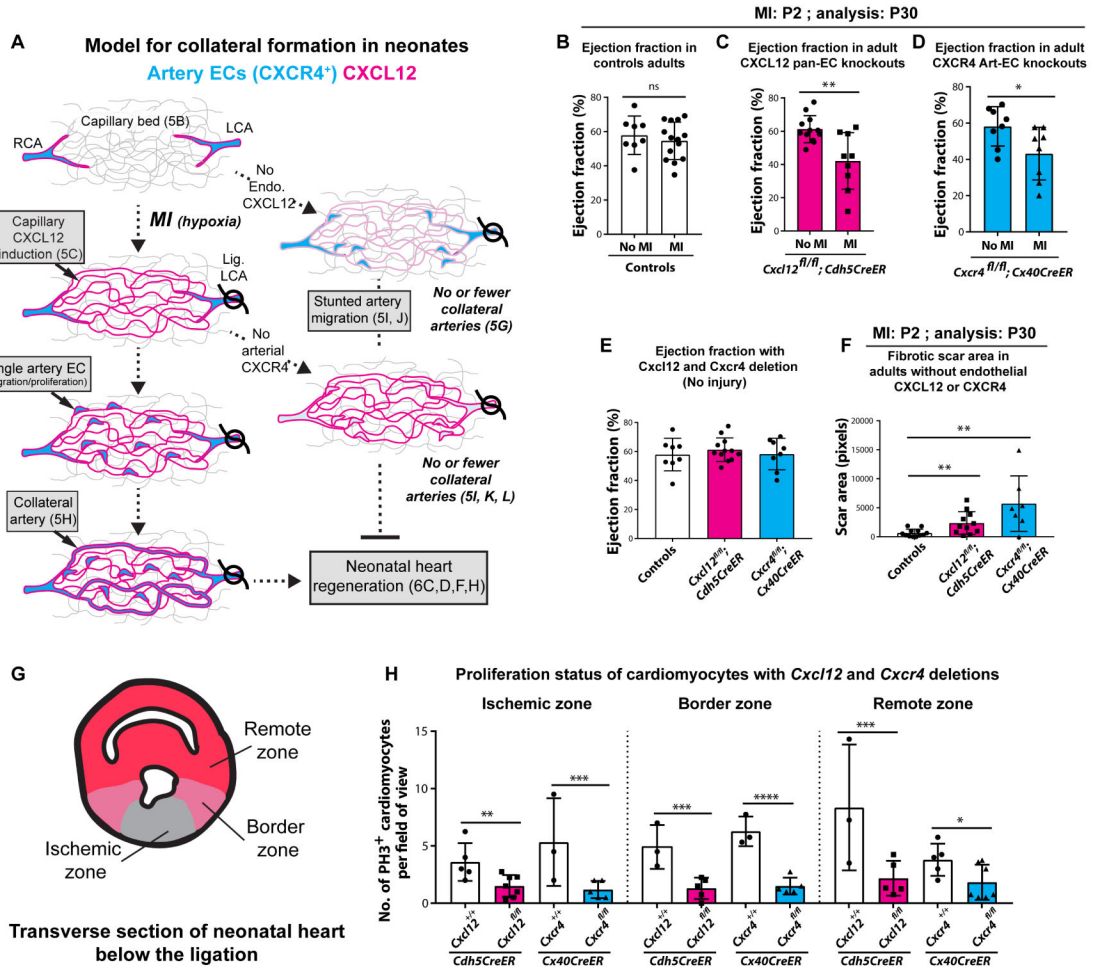

Figure 6. Endothelial *Cxcl12* and *Cxcr4* facilitate neonatal heart regeneration. See also Figure S5 and S6.

(**A**) Model for collateral formation in neonates upon MI. (**B**-**E**) Ejection fractions 28 days post-MI. No decrease in controls (**B**) (n=8 No-MI, n=14 MI animals). Function is reduced with Pan-EC *Cxcl12* deletion (**C**) (n=12 No-MI, n=9 MI animals) and arterial *Cxcr4* deletion (**D**) (n=8 No-MI, n=8 MI animals) 28 days post-MI. (**E**) Normal function in non-injured hearts with postnatal endothelial gene deletions. N= 8 controls, n=12 *Cxcl12$^{fl/fl}$; Cdh5CreER*, n=8 *Cxcr4$^{fl/fl}$; Cx40CreER* animals. (**F**) Compared to controls (n=12), fibrotic scar was increased in endothelial *Cxcl12* (n=11 hearts) and arterial *Cxcr4* (n=7 hearts) knockouts. (**G**) Transverse section indicating ischemic zone, border zone and remote zone. (**H**) Reduced PH3^{+} cardiomyocytes in ischemic, border, and remote zone of neonatal hearts lacking endothelial *Cxcl12* (n≥5) or arterial *Cxcr4* (n=5), 7 days post-MI. lig, ligated; LCA, left coronary artery; RCA, right coronary artery; P, postnatal; Endo, endothelial; EC, endothelial cell; MI, myocardial infarction. Error bars are st dev: *, p≤0.05; **, p≤0.01; ***, p≤0.001, ****, p≤0.0001.

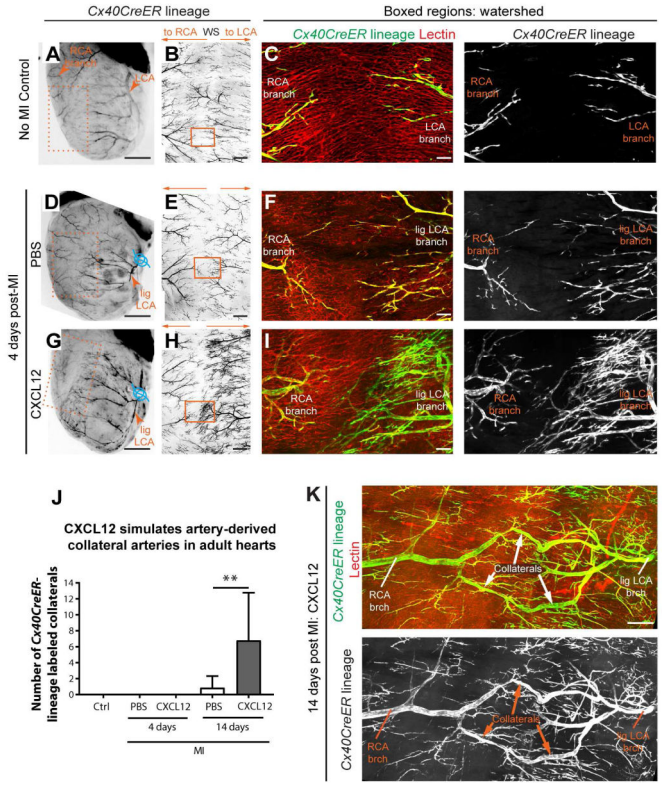

Figure 7. CXCL12 administration induces collateral formation through Artery Reassembly in adult hearts. See also Figure S7.

(**A**, **D**, and **G**) Stereoscope images of adult *Cx40CreER; Rosa26*^{TdTomato} hearts. Arterial endothelial cells, black; ligation, blue. Tamoxifen given 2 days before MI; heart isolated 4 days post-MI. (**B**, **E**, and **H**) Confocal imaging of isolated anterior heart walls (boxes in **A**, **D**, and **G**) showing left (LCA) and right (RCA) coronary artery branches in watershed (WS). (**C**, **F**, and **I**) Boxed regions in **B**, **E**, and **H** showing *Cx40CreER*-lineage and perfused Lectin. CXCL12 increases artery cell outgrowth from LCA branches. (**J**) CXCL12 treatment induced artery-derived collaterals at 14 days post-MI (from left to right: n=4, n=5, n=10, n=13, and n=14 hearts). (**K**) Artery-derived collateral from CXCL12 administered heart Ctrl, control; Lig, ligated; MI, myocardial infarction; brch, branch. Scale bars: **A**, **D**, and **G**, 2 mm; **B**, **E**, and **H**, 500μm; **C**, **F**, and **I**, 100μm; **K**, 200μm. Error bars are st dev: **, p≤0.01.